STRATOFLY MR3 – how to reduce the environmental impact of high-speed transportation

Nicole Viola, Roberta Fusaro and Oscar Gori
Politecnico di Torino, c.so Duca degli Abruzzi 24, 10129 Turin, Italy
Marco Marini, Pietro Roncioni and Guido Saccone
CIRA (Italian Aerospace Research Centre), Via Maiorise snc, 81043 Capua (CE), Italy
Bayindir Saracoglu, Ali Can Ispir
von Karman Institute for Fluid Dynamics, Rhode-Saint-Genese, Vlaams-Brabant, B-1640, Belgium
Christer Fureby, Thommie Nilsson
Lund University, Faculty of Engineering, Lund, PO Box 118, SE 221-00, Sweden
Christian Ibron, Niklas Zettervall, Kevin Nordin Bates
The Swedish Defence Research Agency, FOI, Stockholm, SE I64 90, Sweden
Axel Vincent
ONERA, Palaiseau, 91120, France
Jan Martinez-Schram
German Aerospace Center, Göttingen,37073,Germany
Volker Grewe, Johannes Pletzer
DLR-Oberpfaffenhofen, Institut für Physik der Atmosphäre, Wessling, 82234, Germany
Didier Hauglustaine
Laboratoire des Sciences du Climat et de l'Environnement (LSCE), Centre National de la Recherche Scientifique (CNRS), 91191 Gif-sur-Yvette, 91191, France
Florian Linke, Daniel Bodmer
Institute of Air Transportation Systems, Blohmstr. 20, 21079 Hamburg, Germany

Abstract

This paper addresses the main progresses and achievements of the H2020 STRATOFLY Project, funded by the European Commission, under the Horizon 2020 framework, specifically looking at the latest results in terms of environmental sustainability. In particular, starting from reporting the main environmental challenges posed by high-speed civil transportation, at local, regional and global levels, this paper describes the way in which the STRATOFLY MR3 vehicle, a Mach 8 waverider fueled with liquid hydrogen, promises to limit the overall environmental impact. In details, firstly, the paper describes some of the main technological improvements adopted to reduce the aircraft emission and then it reports about the status of the numerical and experimental test campaigns on the high-speed engine, showing the results achieved so far. This preliminary emission inventory allows for the evaluation of emission indexes throughout the mission profile, the verification of the compliance with the ICAO prescriptions, the estimation of the impact on air quality and climate and eventually, when necessary, the paper proposes adequate mitigation actions.

I. Introduction

Currently, a worldwide growing attention to dramatically reduce the environmental impact of civil aviation in the next decades is clearly visible. At the same time, the willingness to improve the current civil transport aircraft performance is also urging the scientific and engineering community to foster international cooperation with the final goal of developing new high-speed vehicles. The idea of covering long-haul routes in some hours (one order of magnitude shorter with respect to the current civil transportation) fascinates the aviation sector, with promising business cases. In parallel, the research activities in the field of hypersonic transportation system are also pushed by the space sector because the development of key enabling technologies for the hypersonic flight may be a preparatory step towards the development of future reusable access to space systems. In summary, this worldwide incentive to consider commercial high-speed transport, is particularly urging Europe to quantitatively assess the potential of civil highspeed aviation with respect to technical, environmental and economic viability in combination with human factors, social acceptance, implementation and operational aspects.

As eluded in previous studies, with special reference to those carried out in the European framework, some innovative high-speed aircraft configurations have now the potential to assure an economically viable high-speed aircraft fleet. Investigations carried out in more than a decade of EC- supported research projects have permitted maturing a number of configurations leading to the airframe-integrated propulsion concept: ATLLAS I/II [1], LAPCAT I/II [2], HIKARI [3], HEXAFLY [4], HEXAFLY Int. [5]. They make use of unexploited flight routes in the stratosphere, offering a solution to the presently congested flight paths while ensuring a minimum environmental impact in terms of emitted noise and green-house gasses, particularly during stratospheric cruise. Only a dedicated multi-disciplinary integrated design approach could realize this, by considering airframe architectures embedding the propulsion systems as well as meticulously integrating crucial subsystems. In this context, starting from an in-depth investigation of the current status of the activities, the STRATOFLY project has been funded by the European Commission, under the framework of Horizon 2020 plan, with the aim of assessing the potential of this type of high-speed transport vehicle to reach TRL6 by 2035, with respect to key technological, societal and economical aspects. Main issues are related to thermal and structural integrity, low-emissions combined propulsion cycles, subsystems design and integration, including smart energy management, environmental aspects impacting climate change, noise emissions and social acceptance, and economic viability accounting for safety and human factors.

In this paper, the main environmental challenges posed by high-speed civil aviation are discussed together with the main goals set by ICAO for the next decades (Section III). Then, Section IV thoroughly describes the multidisciplinary methodology defined in the framework of the H2020 STRATOFLY project, with the aim to assess the environmental sustainability of its high-speed vehicle and mission concepts. In details, keeping the available ICAO regulation as a starting point, different algorithms have been developed to evaluate emissions produced during LTO (Landing and Take-Off) cycles as well as those produced during the CCD phases (Climb-Cruise-Descend). These algorithms will combine the results coming from both the numerical and the experimental test campaigns carried out in the project.

Therefore, after depicting the integrated methodology, the Section provides an update on the status of the numerical and the experimental test campaigns, also providing the readers with a set of preliminary results, when available. Finally, Section IV reports an updated schedule foreseen for the implementation of the methodology. Then, Section V describes the way in which numerical and experimental results are

processed to generate representative emission inventories to be then exploited to estimate Air Quality and Climate Impact. As thoroughly described in the Section, the algorithms developed within the H2020 STRATOFLY Project aim at assessing the environmental sustainability of the defined concept at local, regional and global scales. Eventually, main conclusions are drawn and ideas for future works are reported.

II. Sustainable high-speed civil aviation: main challenges and goals

According to the ICAO 2019 Environmental Report,

> *Aviation is in essence a technology-driven sector that has fulfilled humankind's dreams of flying. The next chapter for aviation will be to fulfil the societal aspiration of an environmentally sustainable flying future. The fourth industrial revolution offers an enormous opportunity, and innovation is at the forefront of the breakthrough needed to deliver fully sustainable air transport.*

Perfectly in line with this idea, STRATOFLY Project, since its conception, has decided to focus not only on the major technological challenges posed by the high-speed flight, but also to address the most relevant operational challenges. In particular, one of the most ambitious goal of the project is the reduction of the climate impact, by pursuing pollutant and greenhouse gases emissions abatement to comply with current and future expected prescriptions for subsonic civil aircraft. While such ambition was barely unrealistic at the time of Concorde supersonic transport, the technology steps forward and the high levels of integration of the propulsive system within the airframe currently pave the way towards the design of high-efficient vehicles and low-emissions combustors.

A. Main Environmental challenges of high-speed aviation

ICAO Assembly Resolution A39-1 instructs the Council to ensure that they take due account of the problems that the operation of supersonic aircraft may create for the public, which may be classified as at airport/local and global level. At airport/local level jet–noise and pollutant emissions play a crucial role to determine noise emissions and air quality that may affect airport personnel working in the area, passengers travelling and people living nearby. At global level sonic boom, and pollutant and greenhouse gases emissions need to be considered to determine respectively noise annoyance to people living in the areas overflown by the airplanes and the impact on climate. Both noise emissions and pollutant emissions can be a serious showstopper for high-speed flight, unless both the design and the operations of high-speed aircraft can solve the open environmental issues.

B. Main Environmental goals of high-speed aviation

Considering that the most ambitious goal of high-speed aviation consists in targeting the same levels of emission of civil subsonic aviation, in the full-length paper, this Section will present and discuss the ICAO regulations and guidelines in the field of environmental impact, specifically looking at the following reference documents:

- ICAO, "Annex 16 Volume I: Aircraft Noise" [6]
- ICAO, "Annex 16 Volume II: Aircraft Engine Emissions" [7]
- ICAO, "Annex 16 Volume III: Procedures for the CO2 Emissions Certification of Aeroplanes [8]

III. STRATOFLY MR3 – numerical and experimental emission inventory

A. Methodology Overview

Figure 1 shows the overall methodology for environmental impact evaluation. Starting from the design of the vehicle and its concept of operations, numerical simulations coupled with test campaigns generate emission indices throughout the mission. It is worth highlighting that while test campaigns focus on supersonic combustion and therefore specifically on the operations of the DMR (Dual Mode Ramjet) engine, numerical simulations cover a wider spectrum of operations, including the ATR (Air Turbo Rocket) engine and the ATR-DMR transition. Emission indices are fundamental to generate the 3D emission inventories, which are crucial to optimize the trajectory and subsequently to estimate the impact on climate and air quality. Eventually, the methodology allows comparing the results with
current regulations and, in case of not compliance, may suggest modifications. The main outcome of the methodology is therefore the assessment of the environmental compatibility of the high-speed vehicle under investigation. However, the application of the methodology to STRATOFLY MR3 can be useful also to develop new algorithms for emission estimation in conceptual design to verify the compliance with the environmental requirements at a very early stage of the design process.

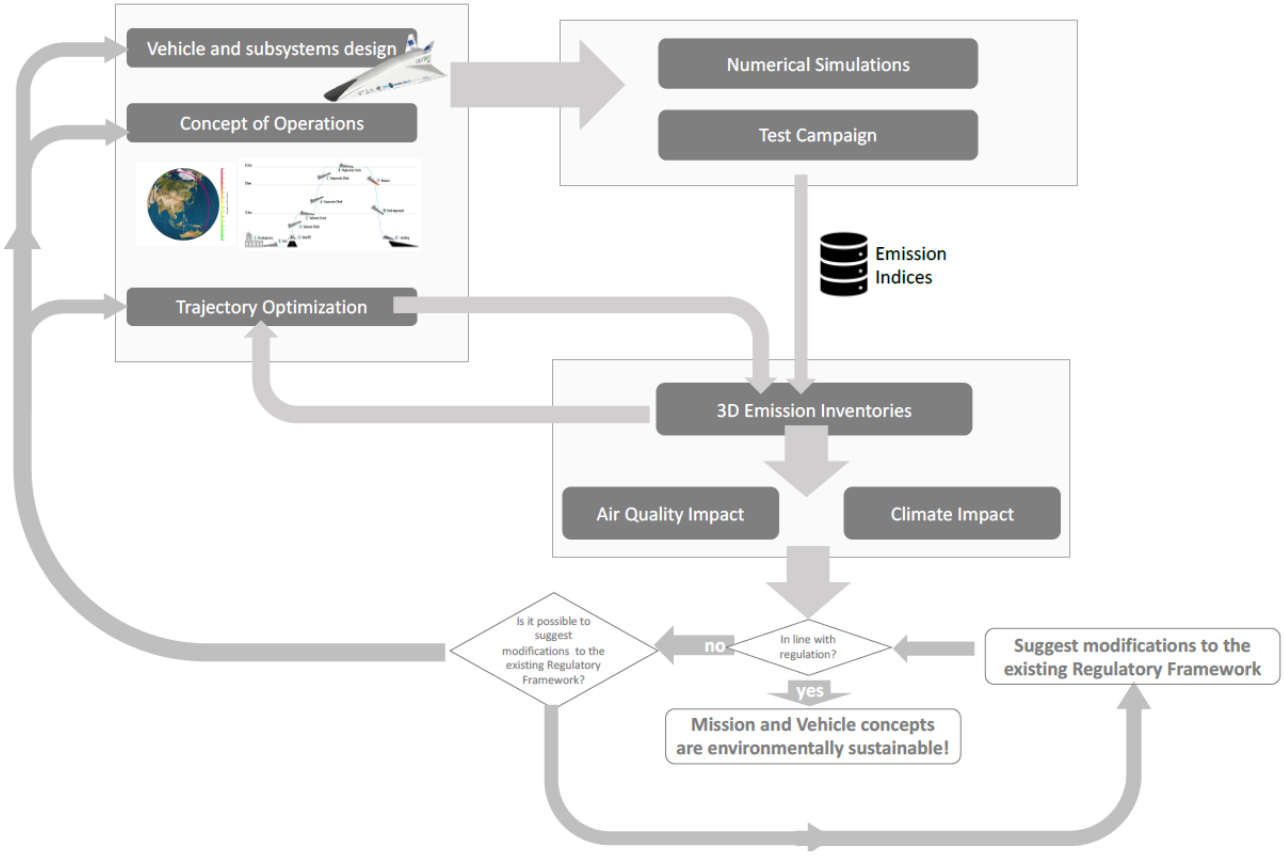

Figure 1. Methodology for environmental impact

B. STRATOFLY MR3: Aircraft and Subsystems performance

STRATOFLY MR3 is the hypersonic vehicle for civil passenger transfer flying at Mach 8 during cruise in the stratosphere which is focus from both the design and operations point of view of the STRATOFLY project [9]. The vehicle configuration is currently under development (see Figure 2). This vehicle shall be capable of flying at Mach 8 in cruise at an altitude of 30 – 35 km carrying 300 passengers over antipodal

routes (>18000 km range). The vehicle uses a dual propulsion plant based on air-breathing engines composed by six Air Turbo Rocket (ATR), to power the vehicle up to Mach 4.5, working as turbo rocket in subsonic condition and as ramjet in supersonic regime, and one Dual Mode Ramjet (DMR) which is ignited in hypersonic speed regime and works initially as ramjet first, switching then to scramjet mode up to Mach 8. Engines use liquid hydrogen as propellant.

Figure 2. STRATOFLY MR3 vehicle

Overall vehicle characteristics are reported in Table 1.

Table 1. STRATOFLY MR3 aircraft specifications

Parameter	Value	Unit of Measure
Length	94	m
Wingspan	41	m
Wing surface	1365	m^2
Aspect ratio	~1	-
MTOW	400000	kg
OEW	190000	kg
Payload (300 pax @ 100 kg)	30000	kg
Fuel Capacity	180000	kg
Cruise Mach	8	-
Service Ceiling	35000	m
Range	18700	km
ATR engines thrust @ sea level (total)	3000	kN
ATR engine thrust @ BOC supersonic (total)	2800	kN
DMR engine thrust @ BOC hypersonic	500	kN
DMR engine thrust @ hypersonic cruise level	1033	kN

The aerodynamic work on STRATOFLY MR3 has started from the LAPCAT-II MR2.4 vehicle aerodynamic database [2], and is taking into account the geometrical modifications which step-by-step are being introduced during the configuration evolution. Aerodynamic performance of MR3 is analysed, for external surfaces only (no propulsive flowpath), from Mach=1.5 to Mach=8 by using CIRA's surface impact method [11], and for the whole Mach number regime (from Mach=0.3 to Mach=8) by inviscid CFD simulations by both CIRA and POLITO. Clean configuration as well as the effect of the different aerodynamic control devices (elevons, rudders, canard wings, body-flaps) are analyzed in detail,
so defining the proper aerodynamic database based on the classical building-up approach. Then, in order to use this aerodynamic database for trajectory calculations, the different corrections must be applied in

the trajectory design loop: i) viscous axial force correction, ii) spillage lift correction, iii) internal propulsive flowpath corrections in engineoff conditions, iv) installed net thrust in engine-on conditions (already depurated by intake drag, internal engine drag and spillage drag), and v) pitching moment correction due to installed net thrust (beneficial engine-on effect on pitching moment coefficient with a shift-up of the curve).

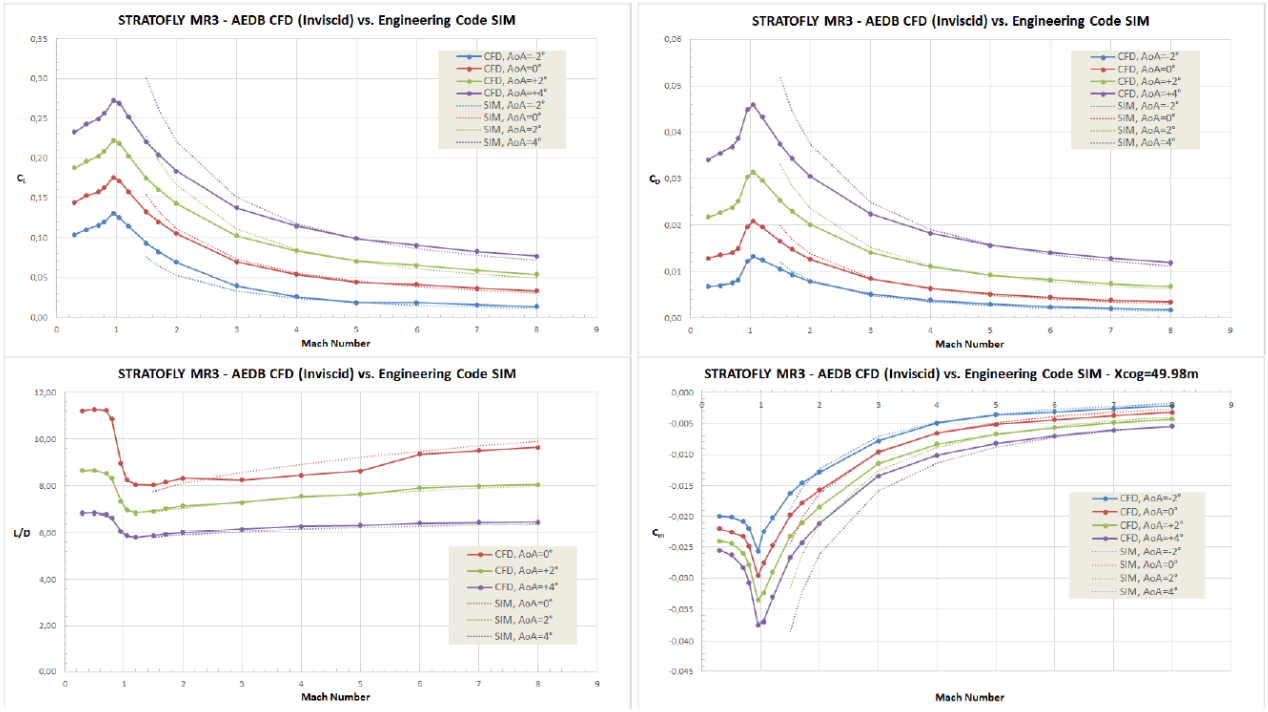

Figure 3. MR3 Aerodynamic characteristics: lift coefficient (top left), drag coefficients (top right), aerodynamic efficiency (bottom left) and pitching moment coefficient (bottom right)

Figure 3 describes the aerodynamic performance of the MR3 vehicle, in terms of lift, drag and pitching moment coefficient (with CoG at 53%), and aerodynamic efficiency. A linear behavior of lift coefficient in the AoA range is predicted at all Mach numbers as well as a high lift-to-drag ratio at AoA=0° (about 10 at Mach=8 cruise condition), as expected by a waverider configuration. Please, consider that the aerodynamic efficiency is reduced enough due to viscous and internal flowpath effects; as a reference, the viscous nose-to-tail CFD simulation of MR2.4 configuration at Mach=8 cruise condition provided a lift-to-drag value at AoA=0° in the range 6.6÷6.9 to be compared with 9.65 of the inviscid CFD simulation of MR3 configuration (external surfaces only). Moreover, Mach number independence of aerodynamic coefficients is still not fully reached at Mach=8, and it appears also that engineering methods and low fidelity CFD results produce very similar results only for Mach number higher than 4. A clear longitudinal static stability ($Cm\,\alpha < 0$) at all Mach numbers is also predicted, with a decrease of stability with Mach number and with more backward CoG. It is also clear the need for longitudinal trimmability with negative elevon deflection for all flight conditions (large ΔCm to null, greatest for Mach around one), thus confirming the conflicting requirements: stability vs. trimmability. Moreover, the MR3 vehicle clearly features a lateral-directional static stability [10], which however decreases with Mach number and is not affected by the AoA range variation, and with a very small effect of CoG movement on lateral stability.

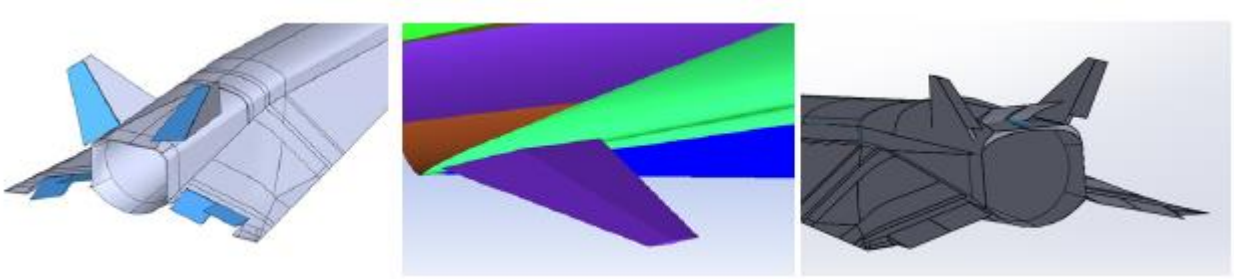

Figure 4. MR3 Flight Control System: elevon and rudders (left), canard wings (center) and extended elevons and body-flaps (right)

As far as longitudinal trimmability map is concerned, possible viable solutions investigated to get trim conditions for optimum propulsive thrust and maximum aerodynamic efficiency (i.e. avoiding approaching the limits of deflection range for all control surfaces, see Figure 4) are: i) exploit the beneficial effect of engine-on, ii) consider the effect of frontal canard wings, iii) extend the chord of the elevons (cantilevered, with same hingeline), iv) add a couple of body-flaps in the rear upper part of the fuselage. The propulsion plant of STRATOFLY MR3 aircraft is a combination of two different engines; air turbo rocket engine (ATR) that is rocket based air-breathing engine and dual mode ramjet engine (DMR) which can be operated in both ramjet and scramjet modes. There are six ATR engines distributed 3 by 3 on both sides of the DMR duct which is located on the dorsal axis of the aircraft. The ATR engines are responsible to propel the aircraft from take-off till high-supersonic cruise speed which is up to Mach 4.5. The DMR engine kicks in the system beyond cruise speed of Mach 1.5 at ramjet mode to contribute the thrust level during the supersonic acceleration. After cruise speed of Mach 4.5, ATR engines are shut down and the aircraft is only being propelled by DMR engine. The incoming air is taken inside the propulsion duct from the common truncated Busemann type intake, then it is split up by two; core flow goes to DMR engine combustor and other part passes to ATR engines bay. After incoming
air is burned with Hydrogen fuel in the DMR combustor section, the exhaust gas is ejected in the common nozzle section. The air ingested by the ATR engine bay is also by-passed to the common nozzle, after burned also with Hydrogen at ATR combustor, generate thrust [31]. The general schematic of the engine scheme is demonstrated in Fig. 5. The performance of the ATR and DMR engines along the flight trajectory has been determined by one-dimensional thermodynamic simulations. The engine schemes based on flight regime were created in Ecosimpro software which is an object-oriented multidisciplinary simulation platform [32] [33]. The 1D simulations done for several cruise speeds in Ecosimpro were coupled with an in-house optimizer (Computer Aided Design Optimization - CADO [34])
to maximize the engine performance parameters such as thrust, specific thrust and specific impulse while minimizing the fuel consumption and respecting the thrust requirements imposed but the flight trajectory. Not only the operational and boundary conditions of the engine were optimized by this means, but also the emission values were minimized by maximizing the specific impulse.

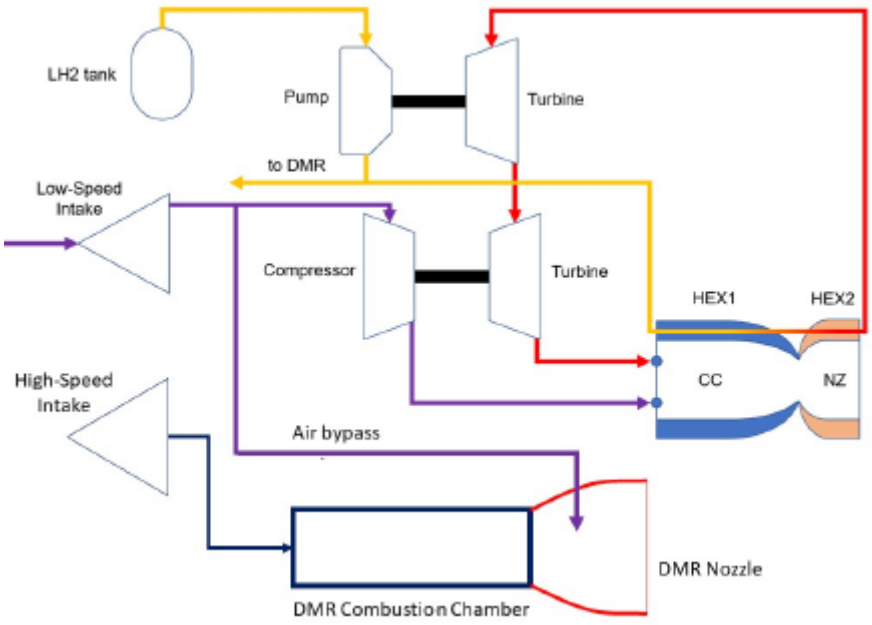

Figure 5. The schematic of the propulsion plant

C. STRATOFLY MR3: Concept of Operations

The original vehicle concept, as well as reference mission Brussels – Sydney, were conceived within the EC funded project LAPCAT II [11] and detailed in STRATOFLY. The original mission adopted for this work is represented in Figure 6. After take-off, the aircraft flies through subsonic climb and cruise, supersonic climb, supersonic cruise with ignition of DMR and switch-off of the ATR engines, hypersonic climb and cruise.

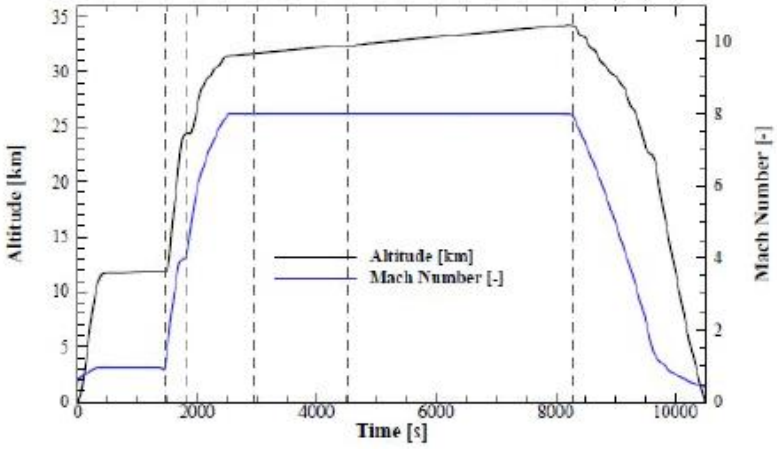

Figure 6. STRATOFLY MR3: nominal flight mission

D. LTO emissions (numerical simulations only)

The engine performance was investigated at the landing and take-off phase in 1D numerical simulations in Ecosimpro. Three speeds of Mach 0.3, 0.44 and Mach 0.5 were selected for this study and design variables were optimized for these conditions. The EINO values and NO production rate were calculated (Fig. 7). The NO production of the ATR engine bay is slightly higher than CFM56 engine during the take-off and climb periods of the LTO phase [35]. However, it is worth noting that the compared value of the engine bay is the sum of six air turbo rockets' emission values. In addition, although the NO production rate increases when the aircraft speeds up, EINO value decreases till the cruise speed of Mach 0.44 due

to the fact that the fuel consumption was optimized as a higher value for this flight speed in order to satisfy trajectory thrust requirement.

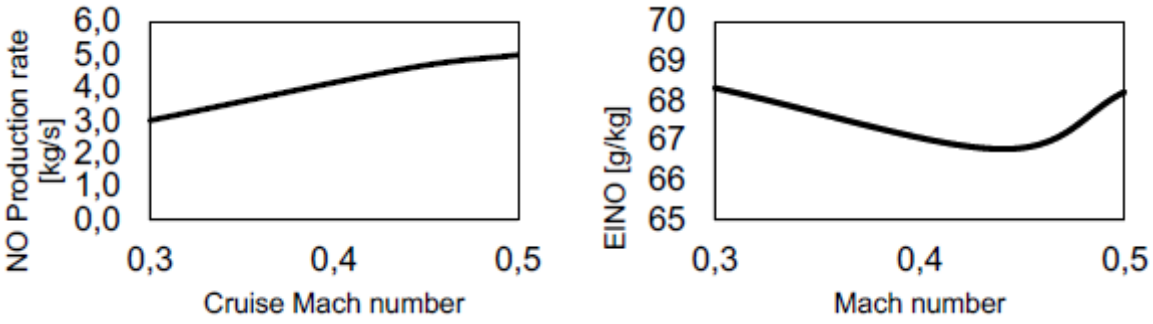

Figure 7. NO production and EINO values during the take-off and subsonic climb of LTO phase

E. CCD emissions (numerical simulations and experimental results)

A generic dual mode ramjet combustor was designed already during the LAPCAT II project [12], with the intent of being able to characterize different operating conditions and associated combustion modes in detail. A schematic of the facility and combustor is shown in Figure 8. The reference position x=0 m corresponds to the throat of the Ma=2.0 nozzle. Hydrogen (H_2) was injected at sonic velocity both from the upper and lower combustor walls at x=0.20 m through two flush-mounted 2.0 mm porthole injectors. The operating conditions considered are 1280 K<T_0<1800 K, where T_0 is the total temperature, and 0.10<f<0.28, where f is the equivalence ratio for a total pressure of p_0≈0.40 MPa. The inflow air-heating was achieved by H_2-air combustion combined with oxygen replenishment. Combustion luminosity, OH* chemiluminescence, wall-pressures, and Schlieren images provide information about the flow physics and flame stabilization mechanisms, and how these parameters vary with operating conditions. The shock-structure and boundary layer separation are found to be sensitive to T_0, and appear to dominate the ignition and flame stabilization mechanisms as seen in Figure 8. The flow along the combustor is overexpanded, and the transition from supersonic to subsonic flow occurs in the downstream section of the combustor (more specifically in the third com-bustor section) approximately between x≈0.75 m and 0.80 m.

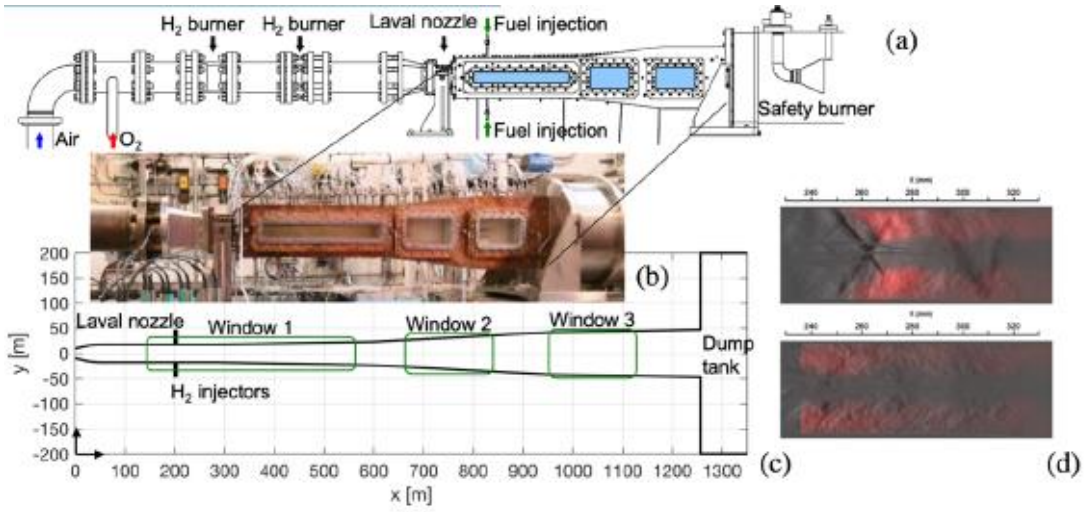

Figure 8. a) General plan of the ONERA LAERTE facility with the LAPCAT-II combustor, b) photo of the LAPCAT-II combustor attached to the ONERA LAERTE facility, c) schematic of the LAPCAT-II combustor, and d) combustion luminosity image of (top) combustion at T0=1414 K and (bottom) combustion at T0 = 1505 [12]

The range of observed combustion modes and flame stabilization mechanisms are attributed to the stagnation temperature and equivalence ratio, but also the wall-roughness have been found to be influential. Subsonic combustion, supersonic combustion, shock-induced combustion and thermal choking have all been experimentally identified as key modes that occur at different operating conditions, some of which may occur in the STRATOFLY MR3 vehicle at different flight conditions during landing/take-off or during transition between ATR and ramjet, and between ramjet and scramjet operation, or at scramjet cruise conditions. In order to increase our understanding of these phenomena and to provide detail visual information about the physics high-fidelity reacting flow simulations have been performed for a few representative operating conditions as will be described next.

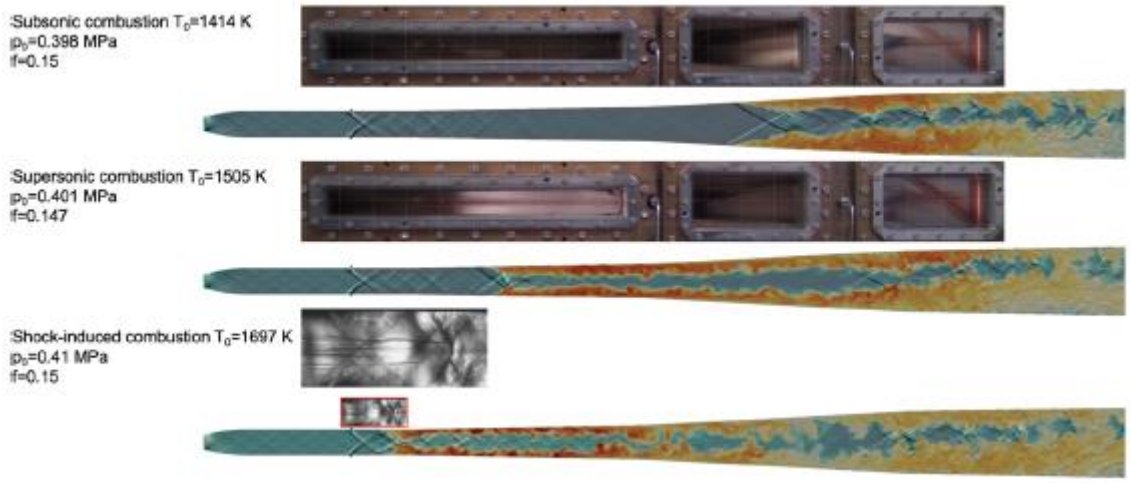

Figure 9. Side view images of the LAPCAT II combustor in terms of numerical schlieren images in gray superimposed by temperature contours for subsonic combustion (top), supersonic combustion (middle) and shock induced combustion (bottom)

Finite rate chemistry Large Eddy Simulations (LES), [13], using the comprehensive H_2-air reaction mechanism of Zettervall *et al.*, [14], the Localized Dynamic K-equation Model (LDKM), [15], and the Partially Stirred Reactor (PaSR) model, [16], have been performed for four representative operating conditions including non-reacting, subsonic, supersonic and shock-induced combustion. The specific purpose of these LES computations is to provide a complementary database, supporting the experimental database and to provide further information about the different flame stabilization mechanism observed experimentally and computationally (see Figure 9). The LES-LDKM-PaSR
model equations are solved using a density-based, segregated, compressible, reacting, finite volume code based on OpenFOAM, [17]. The code is second order accurate in both space and time and employs the Kurganov central upwind convection scheme together with a shock-sensor to help determine the location of strong shocks. Moreover, the chemical source terms in the species transport equations are evaluated using an operator-splitting approach together with a stiff Rosenbrock solver, [18]. The code is fully parallelized and scales linearly above 10,000 cores. Figure 9 shows instantaneous numerical Schlieren images in gray superimposed by semi-transparent images of the temperature for subsonic, supersonic and shock-induced combustion, respectively. Hex-dominant computational grids with ~26 and ~77 million cells, using refinement at the walls, are used. Subsonic combustion occurs for low values of T_0, with combustion anchoring in the narrow unsteady recirculation regions formed just after the flow separation in the second divergent channel section. Supersonic combustion occurs for intermediate values of T_0, with combustion taking place after a substantial ignition delay in the upper and lower H_2-enriched jet-wakes.

At higher T_0 shock-induced combustion is observed with combustion taking place behind a lambda-shock structure developing at some distance downstream of the two injectors. Qualitatively the LES results match well with the experimentally observed trends as can be observed from figure 9. More specifically, for T_0=1414 K both the experimental and LES images show that combustion starts in the subsonic region in the third combustor section, just after the 1° to 3° transition (in the second window) at 0.75<x<0.80 m. For T_0=1505 K both the LES and experimental images reveal that combustion occurs earlier, towards the end of the first (straight) combustor section or in the beginning of the second combustor section (first window). Experiments suggests a sharp combustion front located around x≈0.35 m, whereas LES predicts a sharp combustion front somewhat further downstream around x≈0.38 m. For T_0=1697 K both LES and experiments shows that combustion takes place even earlier. The experimental combustion image and the combined OH* and Schlieren images shows that combustion starts abruptly at x≈0.26 m due to the presence of a Lambda shock after which the combustion front anchors. The LES predictions support this observation, clearly revealing the development of a Lambda shock behind which combustion stabilize.
The STRATOFLY MR3 Dual-Mode-Ramjet (DMR) engine used in hypersonic conditions, from the ATR/DMR transition to the Mach 8 cruise, is equipped with a combustor 8 m long and 4 m wide, with a constant area elliptical section, and a struts array arrangement mounted as a reversed-V with respect the flow direction [2]. Figure 10 shows the combustor schematics and dimensions (horizontal section), and some 3D CFD results in terms of static temperature [19]. The main issues of air/hydrogen combustion at stratospheric altitudes are represented by NO_x emissions and unavoidable production of water vapor. Regarding the NO_x emissions, ICAO [7] defined threshold values as function of altitude, which cannot be overcome, so a reliable prediction of NO_x emissions is necessary when designing such hypersonic stratospheric transport vehicles.

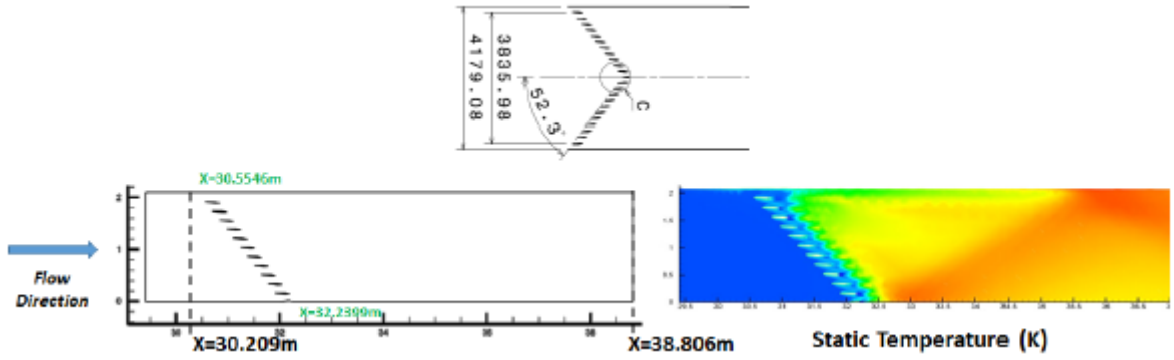

Figure 10. Top view of injector array (top) and half-combustor schematics with CFD temperature (bottom)

Nitrogen monoxide mass fractions, generated by hydrogen/air combustion at the initial operative conditions of STRATOFLY vehicle configurations at three flight speeds i.e., Mach number equal to 4.0, 6.0 and 8.0 were firstly evaluated by an engineering approach. The final conditions of the chemical reacting mixtures, in terms of pressure, adiabatic temperature and NO emission indexes – EINO in perfectly stirred, batch, adiabatic, isochoric reactors were calculated by means of the open-source 0D Cantera software under Python interface. Two different kinetic mechanisms i.e., Zettervall & Fureby [14], labelled as Z25 including also the three fundamental Zel'dovič [20] NO thermal route production steps and Jachimowski detailed – 1988 [21], indicated as JD, were used and the EINO indexes were determined according to the following formula:

$$EINO = 1000 \frac{m_{NO}}{m_{H_2,injected} - m_{H_2}}$$

Furthermore, at Mach numbers ranging from 0.3 up to 3, corresponding to ATR combustion temperatures lower than the auto-ignition points of hydrogen/air reacting mixture (about 845 K at atmospheric pressure), EINO were calculated using a special methodology consisting in modeling start-up of the burning process, by means of a 0D supply of an impulsive energy, simulating an electric spark. Thermal power, width of the energy pulse and time of the heat flux pulse peak were suitably selected in such a way to keep constant the final thermodynamic equilibrium temperatures, achieved by the initial reacting mixtures.

Table 2. Emission indexes of NO and final combustion conditions predicted by 0D simulations at three relevant flight conditions for Dual Mode Ramjet - DMR

Flight Conditions		**Local Conditions@Strut**		
Alti-tude	**Mach**	**Mach**	**P**	**T**
[km]	**[-]**	[-]	[Pa]	[K]
21	**4**	1.36	164538	663.16
26	**6**	2.49	103709	814.66
32	**8**	3.33	57429	963.74

		Combustion Conditions							
Alti-tude	**Mach**	**τ**	**φ**	**Pf [Pa]**		**Tf [K]**		**EINO [gNO/kg H_2]**	
[km]	**[-]**	[s]	[-]	Z25	JD	Z25	JD	**Z25**	**JD**
21	**4**	0.015867	0.80	625576	596622	2872.80	2710.94	**0**	**0**
26	**6**	0.007815	0.70	315510	301275	2785.50	2634.30	**0**	**0**
32	**8**	0.005363	0.65	148665	140792	2782.18	2604.60	**190.70**	**369.45**

Table 3. Emission indexes of NO and final combustion conditions predicted by 0D simulations at low Mach number conditions for Air Turbo Rocket - ATR

			Combustion Conditions					
Mach	**τ**	**φ**	**Pf [Pa]**		**Tf [K]**		**EINO [gNO/kg H_2**	
[-]	[s]	[-]	Z25	JD	Z25	JD	**Z25**	**JD**
0.3	0.0250	0.974	1120495	1128007	2796	2796	**4.45E+00**	**3.78E-01**
0.44	0.0192	0.974	1457239	1462718	2805	2805	**3.51E+00**	**3.43E-01**
0.5	0.0191	0.971	1519710	1528516	2805	2805	**3.57E+00**	**3.41E-01**
0.75	0.0191	0.892	1547837	1554411	2737	2737	**2.69E+00**	**2.22E-01**
0.82	0.0195	0.931	1133796	1137444	2732	2732	**2.94E+00**	**2.38E-01**
1.5	0.0191	0.915	731794	737548	2744	2744	**4.74E+00**	**2.73E-01**
2	0.0185	0.977	764678	771160	2810	2810	**6.28E+00**	**4.20E-01**
3	0.0233	0.909	575345	579145	2842	2842	**1.21E+00**	**7.87E-01**
4	0.1055	0.497	966176	951498	2456	2413	**3.71E+01**	**9.37E+02**
4.5	0.1310	0.779	1653187	1563187	3145	2932	**1.13E+03**	**8.75E+02**

For the low Mach number conditions, the nitrogen monoxide mass fractions were evaluated at the same time instants at which the equilibrium temperatures were reached during a thermodynamic calculation. For Mach numbers equal to 4 and 4.5, at which the initial mixture temperatures were greater than the

auto-ignition points of hydrogen-air and therefore the 0D supply of the energy impulse was not necessary, NO mass fractions were calculated at timeinstants corresponding to the residence times of the flow streams within the STRATOFLY vehicle. Table 2 and Table 3 report the computed results, for the DMR and ATR operative conditions respectively, where in Table 2 the local conditions at struts hydrogen injection have been elaborated based on available nose-to-tail 3D CFD simulations from LAPCAT-II project [2]. In Table 2, for the sake of comparison, the data of zero-dimensional simulations, corresponding to the same residence time τ of the hydrogen/air flow streams within the STRATOFLY vehicle, were considered. It is observed a rather good agreement of EINO value predicted by detailed Jachimowsky scheme at ER=0.65 and at residence time, EINO=370) with the CFD result on 3D full-combustor with reduced Jachimowsky [21], i.e. EINO=450. Moreover, higher pressure and lower temperature conditions (at strut, ahead of hydrogen injection for Mach=4, 6) seem to inhibit the production of NO. In Figure 11 for Mach numbers between 0.3 and 3, the final combustion temperatures using both Z25 and JD kinetic mechanisms are completely superimposed, because they are equal to the final thermodynamic temperatures achieved by the initial reacting mixtures during equilibrium calculations. In this range, EINO predicted by both the kinetic schemes are sufficiently low. At higher Mach numbers i.e., 4 and 4.5, the calculated EINO are significantly greater, but these values are not completely reliable, because the initial pressures are very elevated (respectively, 4 and 6.5 bar) and outside the validity range of the considered mechanisms. The ATR engine performance at speeds of Mach 0.82, 1.5, 2.0, 3.0, 4.0 and 4.5 was investigated for the climb, cruise and descend phases through 1D numerical simulations in Ecosimpro. Additionally, the performance estimations were done along the hypersonic flight trajectory propelled by DMR engine. The EINO calculations and NO production rate were calculated for both ATR (red curve) and DMR engines (black curve) (Fig. 11). The EINO value computed for the simulation of Mach 8 cruise condition are in lined with 0D simulation given in Table 2.

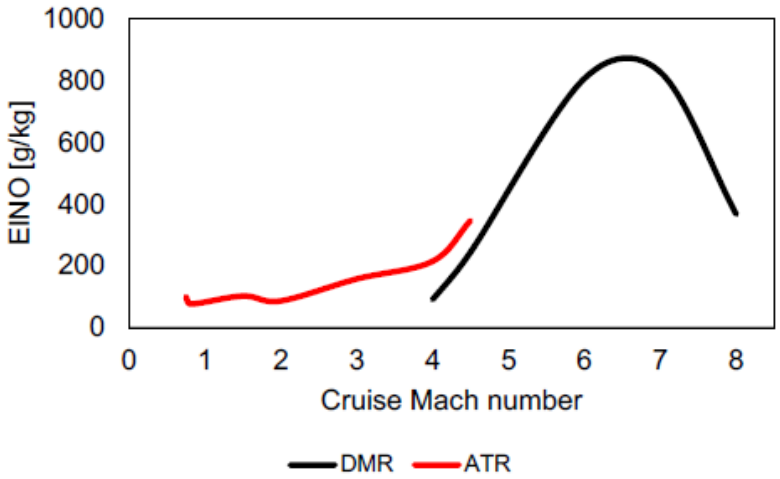

Figure 11. EINO values of ATR and DMR engines during the climb of the CCD phase

In order to support the full-scale RANS described above and to provide more detailed understanding of the dual mode ramjet operation, joint experimental and LES studies have been performed using the Small-Scale Flight Experiment (SSFE) designed to emulate the full-scale STRATOFLY MR3 flight vehicle. In the SSFE a simplified and downscaled version of the flight vehicle was mounted in the DLR High Enthalpy piston-driven shock tunnel Gottingen (HEG), [22] [23]. Figure 12a presents a CAD model of the mounting of the SSFE in the HEG test-section for which free-flight tests were carried out at conditions

corresponding to Ma 7.34 at an altitude of 28 km [24]. The SSFE is suspended in the test-section using two kevlar/aramide cords each of which is arranged in a V-configuration passing through the SSFE and then attached on either side to the clamping mechanism. To allow free flight tests these wires are cut by razor-blades just when the shock enters the test-section, allowing for approximately 4 ms of undisturbed test-time before the SSFE is caught by the model catching mechanism composed of two cylindrical buffers, each mounted between a pair of legs. The SSFE model is rather complex, including a hydrogen injection system and 40 pressure transducers distributed on the intake-, combustor- and nozzle-section. Furthermore, an optical tracking system was installed in the HEG test-section to record the actual displacement of the SSFE model during the free flight tests.

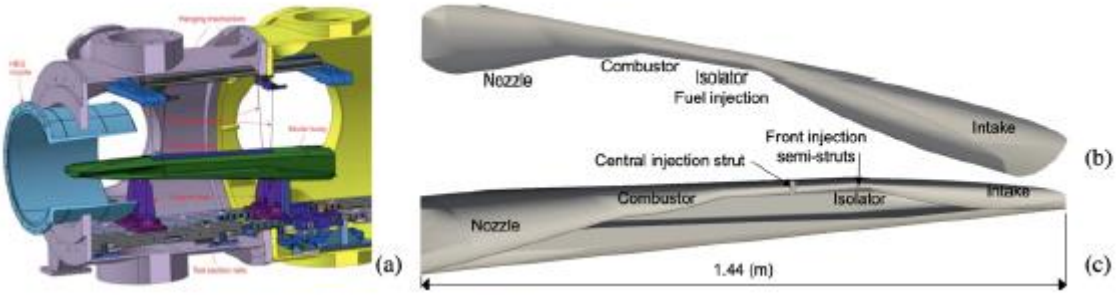

Figure 12. The SSFE. (a) Schematic of the Small Scale Flight Experiment (SSFE) installed in the HEG test section and (b) CAD views of the computational model of the SSFE flight vehicle

Two dual frequency comb lasers at 1760 1/cm +/- 30 1/cm (spectral coverage)@ 0.165 1/cm resolution allow for sampling complete spectra based on a heterodyne signal analysis with acquisition times in the µs – range. This newly development measurement technique is an alternative to TDLAS measurements, which will be applied additionally during the tests. To achieve this 8 measurement points along the flow path in the combustor of the SSFE have been installed in the model. It is foreseen to determine the concentration of water and nitric oxide during the combustion process in a transient mode. LES of the SSFE experiments are underway for two operating conditions, corresponding to the experimental conditions of 27 km and 36 km flight altitude, respectively. The same LES model and H_2-air reaction mechanism as used for the LAPCAT II combustor is used also for the SSFE configuration. A hexahedral dominated grid of ~34 million cells are used for these simulations. This grid is coarse in the freestream but gradually refined towards the SSFE body, with additional refinement along the engine flow path, and in particular towards the SSFE walls, around the semi-struts and the central strut, as well as around the injectors.

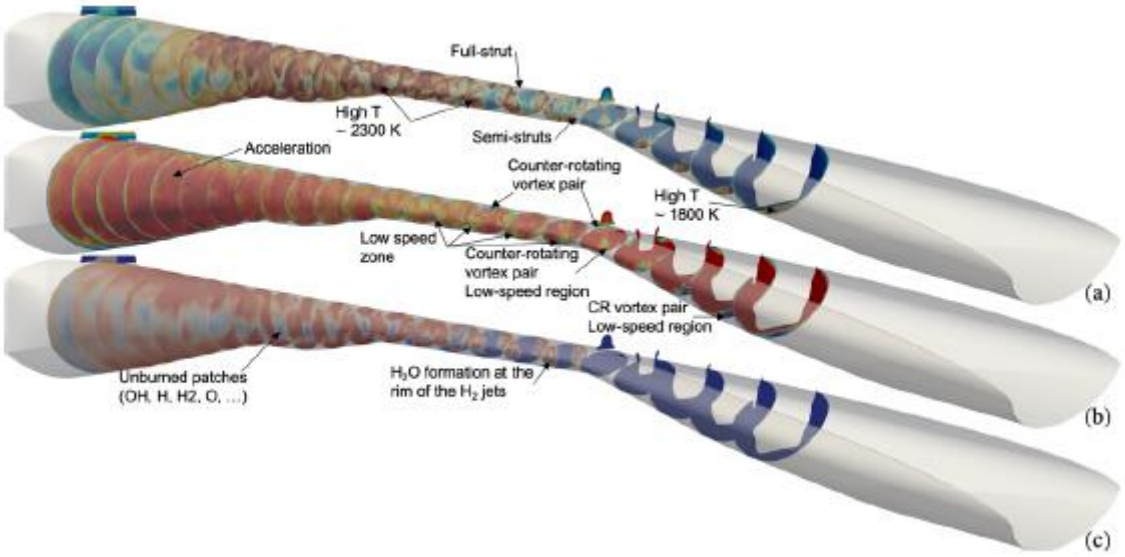

Figure 13. Perspective and side views of flow, mixing and combustion in the SSFE in terms of volumetric renderings of H2 (in pink), temperature (in hot colors) and the Mach number

Figure 13 presents semi-transparent perspective views of the combustor with superimposed LES results in terms of the temperature, T, axial velocity, v_x, and water, H_2O mass fraction to illustrate the flow, mixing and combustion along the full engine flow path. The flow along the intake is very complicated and sensitive to disturbances [25], resulting in the generation of a counter-rotating vortex pair adjacent to the centerline that, in turn, influences the flow and mixing properties further downstream in the combustor. An elongated patch of high temperature air is observed to develop as a consequence of the counter-rotating vortex pair ingesting high temperature boundary layer air into the freestream, reaching all the way up to the combustor entrance. Two large counter-rotating longitudinal vortices develop just after the semi-struts as a consequence of the interactions between the flow over the inlet, including the
counter-rotating vortex pair, the semi-strut wakes, and shear-layers developing around and behind the semi-struts. These counter-rotating longitudinal vortices dominate the while flow in the combustor, creating macroscopic motion driving the microscopic/turbulent mixing. The flow is also influenced by the combustor boundary layer, but more notably by the three-dimensional shock-train that traverses the combustor, the volumetric expansion due to exothermicity from the chemical reactions, and the baroclinic torque and viscous effects. The H_2 is injected from the top of the two semi-struts in the early part of the combustor, and from the four, upper and lower, lateral injectors on the central strut. Self-ignition occurs sequentially: the H_2 injected from the semi-struts ignite halfway between the semistruts and the central strut in the counter-rotating longitudinal vortices but does not lead to complete combustion. The resulting temperature increase is however sufficient to precondition the mixture, which the central strut H_2 is injected into, so that self-ignition occurs almost immediately after the central strut. This combustion front spreads laterally so that most of the remaining H_2 entrained in the counter-rotating longitudinal vortices also ignites and burns. Fully developed turbulent combustion prevail in the combustor, but after 4 ms of simulation time the flow is still evolves. Based on the LES predictions the overall combustion efficiency is estimated to be around 85% for the 26 km flight altitude and is estimated to decrease somewhat for higher altitudes.

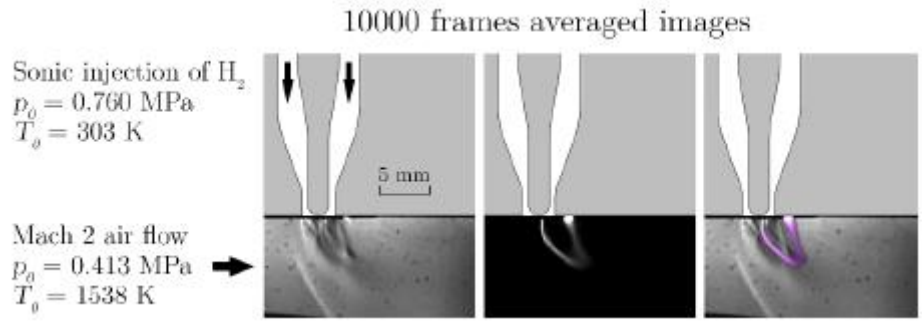

Figure 14. 10000 frames averaged images of: the flow structure in the injection area (Schlieren visualization) on the left, the discharge in the center and the superimposition of them (discharge purple-colored) on the right

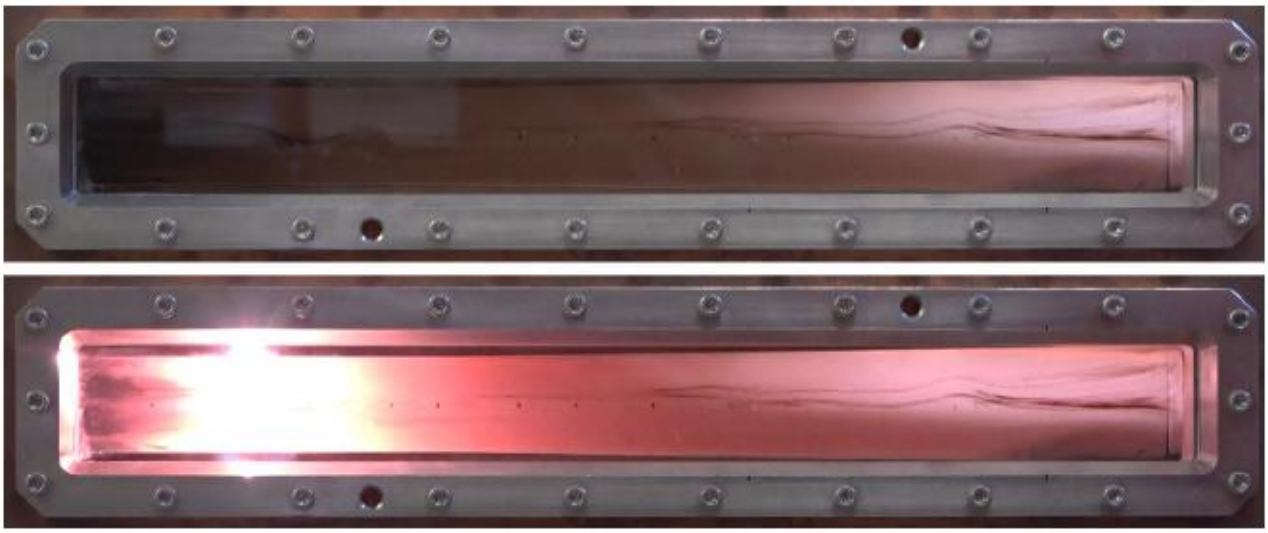

Figure 15. View of the supersonic combustion without plasma (up) and with plasma (down)

Plasma assistance is a promising way to stabilize combustion by preventing unneeded drag. In the European project STRATOFLY, plasma assisted combustion is under investigation to extend the altitude of hypersonic flight, then reducing the environmental footprint of stratospheric emission of water (the photochemical lifetime of water is reduced by a factor of 3 between altitudes of 30,000 m and 35,000 m [26]). In this context, the effect of plasma assistance on supersonic combustion has been experimentally investigated, a quasi-DC discharges [27] being applied to a new design of injector. This fuel injector is fed with a high-speed gas flow which leads the discharge to penetrate the
combustor and the supersonic crossflow. The body of the nozzle-shaped injector is made of metal and connected to the ground whereas a high-voltage electrode is placed at its center with its tip located at the exit of the nozzle, as shown in Figure 13. The combustion experiments were achieved with the LAPCAT2 combustor [28] [29] in the case of a single sonic injection of hydrogen in a Mach = 2 crossflow of hot vitiated air at a temperature close to the self-ignition threshold (T_0 = 1500-1550 K, p_0 = 0.4 MPa). Figure 14 presents flow and discharge visualizations clearly showing the topology of the flow and the path of the filamentary discharge which penetrates the combustor (T_0 = 1538 K, p_0 = 0.4 MPa,
Φ = 0.25). We can remark that the discharge propagates in the hydrogen flow from the tip of the high voltage electrode to its point of maximal extension in the center of the barrel shock structure) and then follows the air/fuel mixing layer to go back to the ground electrode. When a 1.7 g・s-1 hydrogen mass flow (Φ = 0.17) is injected in the supersonic hot air flow, the breakdown voltage occurs around -3.7 kV. As the discharge established between the high voltage and ground electrodes, the voltage drops to about 800 V

and the discharge stabilizes in the arc regime for a current of about 1.8 A (resulting power of 1.4 kW). The plasma is switched off after about 0.9 s. Figure 15 presents images from a camcorder's movie showing the combustion in the first section of the LAPCAT2 combustor less than 1 second before the application of the plasma discharge (upper view) and during the plasma application (lower view). We can remark the strong light emission of the discharge at the injection point. A small increase of the flame's emission is suspected but uncertain due to the possible contribution of the discharge emission
reflected by the rear wall. On the contrary, a significant effect of the plasma on combustion is evidenced with the pressure profile along the combustor (see Figure 16) where a significant pressure increase appears at 300 mm < x < 600 mm. This demonstrates the ability of the quasi-DC discharge generated with this design of plasma assisted fuel injector to improve combustion (higher heat release and then combustion efficiency). As during the run, pressure values can fluctuate, Figure 16 presents average (bold lines) and min/max (normal lines) pressure profiles before plasma application (in blue, for 29.3 s ≤ t ≤ 30.5 s), during plasma application (in red, for 30.7 s ≤ t ≤ 31.3 s) and after plasma application (in
green, for 31.5 s ≤ t ≤ 32.0 s), the reference pressure profile (black line; at t = 27.8 s) being obtained before fuel injection (non-reacting test conditions). At the injection point (x = 200 mm), the shock-induced pressure peak slightly increases during the plasma activation, probably due to the local heating of the flow. At x = 240 mm, the pressure do not vary when the plasma is on, indicating that the discharge do not induce a downstream detachment of the flow. Combustion also seems to start slightly earlier when the plasma is on (300 mm < x < 350 mm).

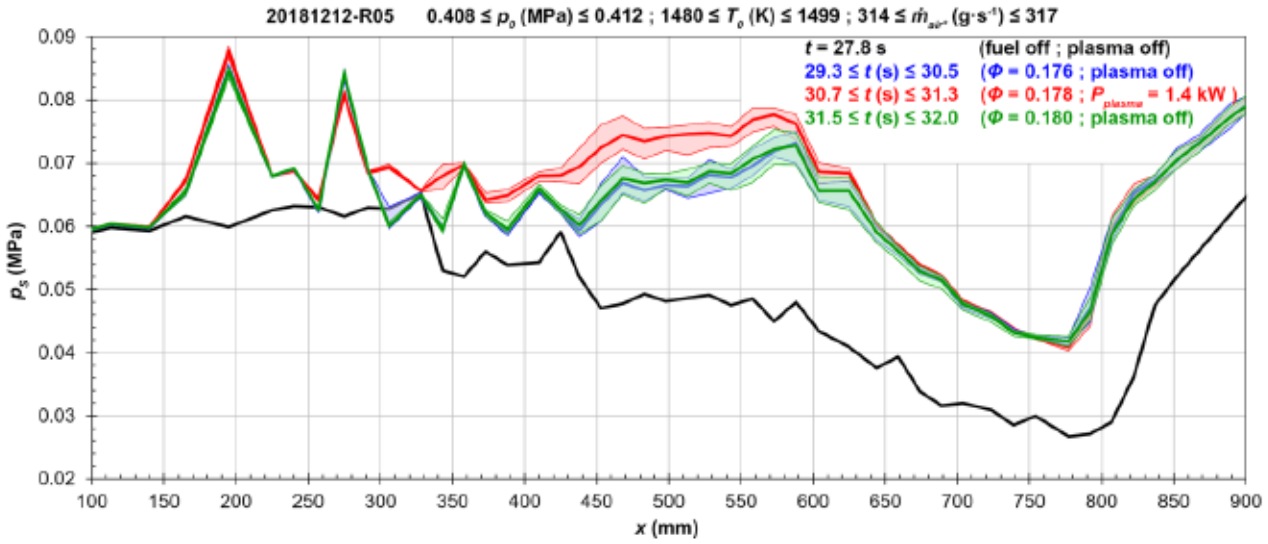

Figure 16. Pressure profile along the combustor before fuel injection (black line) or at phi = 0.18 before (blue), during (red) and after (blue) plasma activation

IV. Atmospheric composition changes and climate impact

A. Emission Inventories

3-dimensional emission distributions are required to determine the changes of the atmospheric composition caused by the STRATOFLY hypersonic vehicle on fleet level and assess the associated climate impact. Those maps or grids of gaseous emissions are often referred to as emission inventories. Based on a network of potential routes, where there is demand and a market to offer hypersonic air transportation, the global emissions from operating the STRATOFLY-MR3 are accumulated and provided as an input for the climate researchers (see sections B., C. and D.). For the calculation of the emission

inventories we use the Global Air Traffic Emission Distribution Laboratory (GRIDLAB). This tool applies a nested trajectory calculator (see also section E.) providing realistic aircraft trajectories
for the hypersonic vehicle designed in the project based on its aerodynamic and engine performance. Typical flight profiles are defined to consider the specificities of hypersonic air travel (e.g. high cruising altitude, acceleration/deceleration segments) and synchronized with the lateral flight path described by a sequence of waypoints that are selected such that the sonic boom impact is minimized (e.g. super-/hypersonic over water only). We calculate the emissions along each trajectory by correlating the engine state per time step to the corresponding emission index in the engine emission database created by numerical simulations and experiments (see above). The emission flow per species is calculated by multiplying the EI with the engine fuel flow. The absolute amount of emissions per trajectory segment is then obtained by integrating the emission flow over time. Finally, the resulting emission profile is rasterized into a 3D grid by determining for each segment the ratio within a certain grid cell and assigning the corresponding percentage of emission to the cell. The emissions from all flights in the scenario are then superposed by adding the emissions for a given grid cell.

B. Hypersonic emissions and related atmospheric processes

Hypersonic emissions are deposited into the atmosphere at a very high altitude, well above the tropopause, i.e. in the stratosphere. Here we are considering a two hypersonic aircraft types (ZEHST and LAPCAT) in addition to a reference aircraft. The respective emission scenarios for the combined sub- and hypersonic aviation were developed within the HIKARI project and show for 2050 a market penetration of 9.8% and 26%, different flight altitudes and different overall emissions of CO_2, H_2O, H_2 and NO_x (see Table 3).

Table 4. Characteristics for 2050 aviation for subsonic only (reference) and two hypersonic configurations. Emissions are given in Tg/year for the sum of sub and hypersonic aircraft

	Market penetration	**Hyper-sonic cruise**	CO2	H2O	H2	NO2
Reference	-	-	**11.2**	**5.0**	**0**	**0.072**
ZEHST	**9.8%**	**25 km**	**10.1**	**22.6**	**0.16**	**0.048**
LAPCAT	**26%**	**30 km**	**8.3**	**31.4**	**0.31**	**0.061**

Figure 17 (left) shows the general circulation with a slow upward motion in tropical areas and a downward motion at polar wintertime latitudes. The emitted species are transported with this circulation and experience a chemical transformation and are eventually transported into the troposphere, where they are either recirculated into the stratosphere, washed-out or deposited on the ground. Figure 17 (right) shows how the emitted species would accumulate in the atmosphere, if no loss processes were present (dotted lines). The transport into the troposphere stabilizes the high-altitude perturbation (above 18 km ~ 100 hPa; dashed-dotted lines) after several years in agreement with earlier studies. The losses in the troposphere largely reduce the re-circulation into the stratosphere for both H_2O and NO_y components.

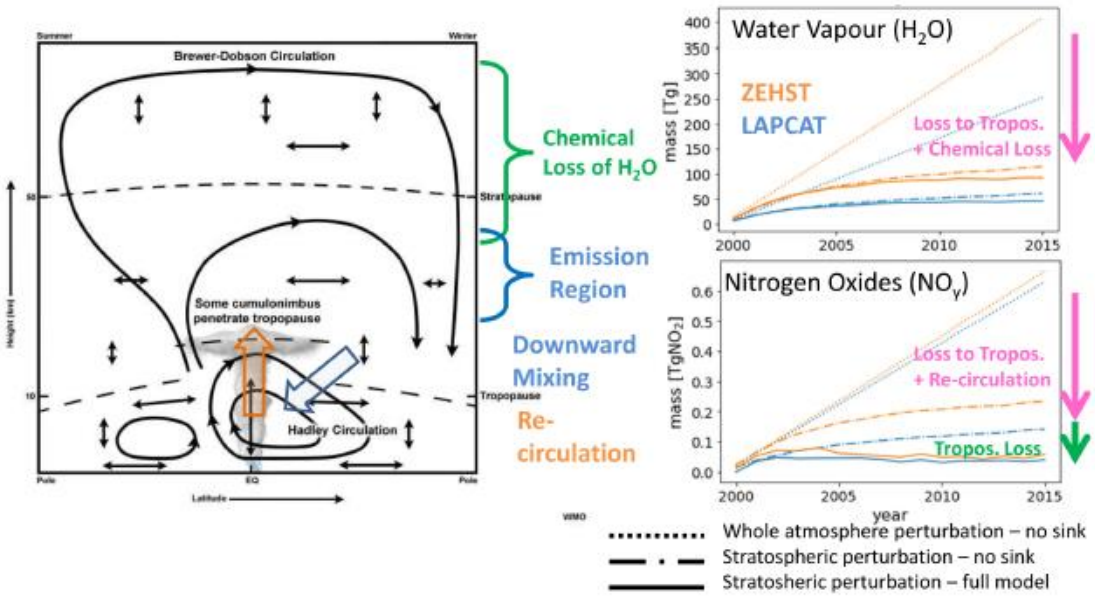

Figure 17. The source of this material (left Figure) is the COMER® Website at http://meted.ucar.edu/ of the University Corporation for Atmospheric Research (UCAR), sponsored in part through cooperative agreement(s) with the National Oceanic and Atmospheric Administration (NOAA), U.S. Department of Commerce (DOC) © 1997-2017 University Corporation for Atmospheric Research

Emitted species accumulate in the stratosphere through different processes:

- H2O:
    - emitted species accumulate in the atmosphere: effective transport into the troposphere limit the accumulation. Additionally, chemical loss occurs (uncertainty see below); (difference between dotted line to dashed-dotted line);

    - re-circulation into the stratosphere is largely limited due to the low temperatures at the tropical tropopause (difference between dashed-dotted and solid line);
- NOy:
    - emitted species accumulate in the atmosphere: effective transport into the troposphere limit the accumulation, despite some recirculation into the stratosphere, which may occur. NOy has no chemical loss (difference between dotted and dashed-dotted line);

    - NOy in the troposphere is washed out via HNO_3 and N_2O_5 and deposite at the ground, which limits a recirculation to the stratosphere (difference between dashed-dotted and solid line).

C. Atmospheric composition changes

The impact of H_2O emitted from hypersonic aircraft will strongly depend on the residence time of water vapour in the stratosphere. The chemical lifetime is dominated by the reaction with atomic oxygen (O_1D). The upward motion will also transport the emitted water vapour to higher altitudes where the H_2O lifetime is much shorter due to additional photolysis by solar radiation (Figure 17). The impact of emissions by the ZEHST fleet on key atmospheric species has been calculated. Water vapour concentrations increase by up to maximum of 640 ppb at 20 hPa at mid-latitudes in the northern hemisphere, which corresponds to the cruise altitude of the ZEHST fleet. Since water vapour is a source of hydrogen radicals, HO_x (=OH+HO_2) increases by up to 10% for this scenario. As a consequence of this increase of HO_x radicals, more HNO_3 is formed and increases by up to 400 ppt (5%). It is unlikely

that the burning efficiency of the fuel is of 100%. Considering that, emissions of H_2 have been included in the set of emissions, corresponding to 10 % of unburnt H_2 fuel. As a consequence, H_2 increases by 60 ppb (7%) due to the direct emissions by the fleet. As a consequence of direct emissions, NO_x increases for this scenario by up to 150 ppt (5%) at the flight altitude of 20 hPa. Due to this increase in NO_x in the stratosphere, the ozone catalytic destruction is enhanced and the O_3 mixing ratio decreases by 40 ppb (-5%). In the lower stratosphere and upper troposphere, the slight increase in NO_x and decrease in HO_x radicals are responsible for a small increase in ozone reaching 6 ppb (0.4%).

Emissions of the LAPCAT hypersonic aircraft have also been used to perform simulations and assess their impact on the atmosphere. The perturbation of the atmospheric species associated to this scenario. Water vapour increases in this case by up to 380 ppb (8%) at 50°N and at the altitude of 10 hPa. The H_2 perturbation reaches 22 ppb (5%). NO_x increases by up to 120 ppt (2%) and consequently stratospheric ozone decreases by about 40 ppb (about -5%) at 5-10 hPa. In the lower stratosphere and upper troposphere, the slight increase in NO_x and decrease in HO_x are responsible for an ozone increase of 5 ppb. As a summary of the chemical perturbations, Table 5 gives the changes in H_2O and O_3 burden, and the change in methane lifetime associated with the change in OH radicals. The increase in H_2O for the ZEHST scenarios is 42. Tg, almost twice the value calculated for the LAPCAT scenario (22 Tg). For ozone, the burden decreases by 4.2 Tg for the ZEHST scenario and by 2.0 Tg for the LAPCAT simulation. The impact on ozone is relatively small but the perturbation is 2 times larger in the case of the ZEHST future fleet than for the LAPCAT case. As a consequence of the increase in OH**,** the methane lifetime decreases by 0.1% in the case of the ZEHST fleet and by 0.05% for the LAPCAT future fleet.

Table 5. Calculated perturbation of the integrated H20 and O3 content in the atmosphere (Tg) and corresponding change in the methane lifetime (%) for the two scenarios

Scenario	ΔH_2O (Tg)	ΔO_3 (Tg)	ΔT_{CH4} (%)
ZEHST	42.2	-4.2	-0.11
LAPCAT	22.4	-2	-0.05

D. Climate Impact

Any climate assessment of new technologies requires a thorough consideration of the underlying objective and underlying scientific question. From that climate metrics, reference and emission scenarios can be easily deduced.

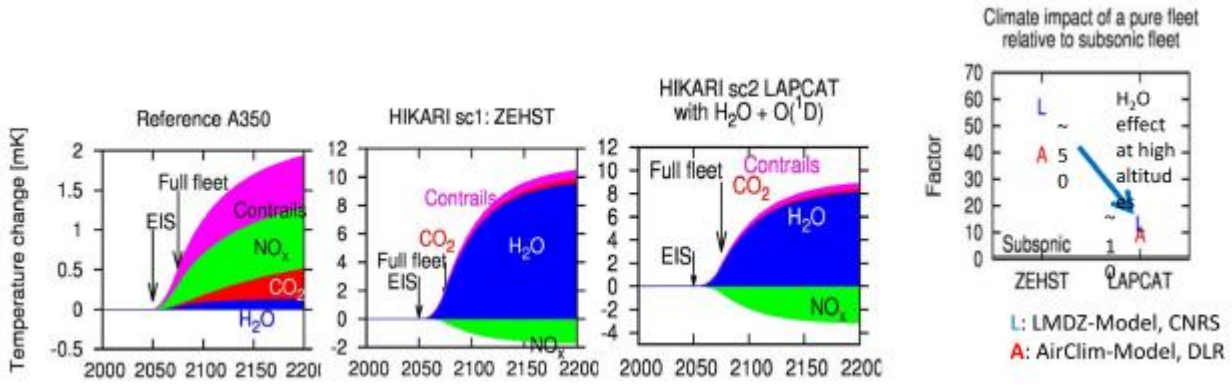

Figure 18. Evolution of the temperature change [mK] caused by the three regarded scenarios (left). And the factor between the climate impact of a HSTC aircraft and a reference aircraft (right)

This clarifies the phrase “climate impact of hypersonic transport” and avoids misinterpretations. The climate question we are posing here is: “How large is the long-term future climate impact if a part of the air traffic is replaced by a hypersonic fleet in comparison to a comparable subsonic counterpart?” Hence we are interested in evaluating different strategies for introducing hypersonic transport, i.e. investigating a whole emission scenario. We are taking into account an entry into service at 2050, with increasing number of flying aircraft up to 2075. At 2075 the considered market penetration is achieved. Long.-term climate impact is interpreted here as the global mean near-surface air temperature change, averaged over the years 2051 to 2150, i.e. a 100-year mean, also called 100 year averaged temperature response (ATR100). Figure 18 shows the climate impact of the 3 regarded emission scenarios. The scenario with subsonic aircraft, only, shows a climate impact via CO_2, nitrogen oxide emissions, and contrails. The hypersonic mixed fleets show a larger impact on climate, basically because of the water vapour emissions in the stratosphere. NO_x emissions in the stratosphere deplete ozone via catalytic reactions. At lower altitudes, e.g. subsonic cruise levels, NOx produces ozone. Both models (LMDz-INCA and AirClim) show the same behavior of ozone depletion at higher altitudes and ozone production at lower altitudes. Ozone depletion leads to a cooling and ozone production to a warming. Both are in the same order of magnitude. LMDz-INCA shows more ozone enhancements than ozone depletion, which results in a warming, whereas AirClim show stronger ozone depletion and hence results in a cooling (shown in Figure 19; green shading). The ratio of the climate impact of the hypersonic mixed fleets to the subsonic only case is shown in Figure 19 (right). Both models agree that the LAPCAT mixed fleet has a lower climate impact (factor 3 to 4 relative to the subsonic only case) compared to the ZEHST mixed fleet (factor 4.7 to 6.5 relative to the subsonic only case). Roughly 90% of the climate impact arises from the water vapour emissions at high altitudes. Note that in this preliminary assessment we have not included the results of the EMAC (DLR) model. The water vapour accumulation is much larger in this model roughly 30% for the ZEHST scenario and a factor of 5 for LAPCAT.

E. Trajectory Optimization for Climate Impact

Trajectory calculators can simulate flight movements and estimate e.g. the associated flight time, fuel consumption and emissions based on aircraft and engine performance models. In STRATOFLY, for this purpose the Trajectory Calculation Module (TCM) [30] is used, which calculates 4D-trajectories, so the aircraft’s position (latitude, longitude, altitude) and states variables as a function of time, based on aerodynamic and engine property databases of STRATOFLY-MR3. Time and locus of an emission are important parameters for the climate impact assessment of the new vehicle, especially with respect to the non-CO_2 effects such as NO_x emissions, water vapour or contrails. By optimizing not only the vehicle from a design perspective but also its flight profile and operating regime a contribution towards minimizing the environmental impact of hypersonic air transport can be made. In a first step, since pollutant gaseous emissions like CO_2, H_2O or SO_2 are approximately proportional to the aircraft’s fuel flow, flight trajectory optimizations regarding a minimum fuel consumption are performed before enhanced methodologies for aircraft emissions distribution analysis or 4D inventory generations shall be applied. Within the scope of this paper, the focus of this subsection is on minimizing the fuel flow of each flight segment, especially within the hypersonic cruise phase as well as in the vertical climb profile. For the latter, the aircraft is forced to dive on a constant energy level within the transonic region (while reaching Mach 1) to obtain an optimum climb path. A fuel-optimal flight level is identified by an exhaustive search algorithm. While

changing the vertical profile definition based on global variables like the hypersonic cruise flight level and simulate a set of different trajectories, an optimum for minimum fuel consumption of the aircraft can be found. This also incorporates a flight controller for keeping an optimal lift coefficient during the hypersonic cruise phase. For the sake of comparability, a flight route
between Brussels and Sydney is chosen for the TCM simulations since detailed reference data of LAPCAT II-MR2.4, the design base of STRATOFLY-MR3, is available for this route [2]. Once the vehicle performance and engine emission data of STRATOFLY-MR3 are available the optimization study will be extended towards the consideration of the climate impact rather than fuel consumption only.

Conclusion

This paper addresses the main progresses and achievements of the H2020 STRATOFLY Project in terms of environmental sustainability. Before entering into the details of the numerical and experimental test campaigns, the paper provides an overview on the main environmental challenges posed by high-speed civil transportation, at local, regional and global levels. In addition, currently available regulations set up by ICAO are analyzed to define emissions benchmarks and references for the future high-speed vehicles. Then, the core of the paper is intended to acknowledge the technical and scientific community on the main technological improvements of STARTOFLY MR3 vehicle to reduce the high-speed aircraft environmental impact and on the status of the numerical and experimental test campaigns on high-speed engines, showing the results achieved so far. Eventually, the emission indices assembled through
low- and high-fidelity numerical simulations (validated for certain phases of the mission by test campaigns) are presented. Future works of the project aim at generating the 3D emission inventories to allow for trajectory optimization and climate impact estimation. The paper ends with a thorough description of the physical phenomena related to highspeed emissions and subsequent atmospheric composition changes, which eventually leads to a complete analysis of the climate impact of high-speed aircraft in a world-wide scenario that encompasses subsonic aircraft. Future works on the estimation of climate impact of STRATOFLY MR3 will follow.

Acknowledgments

This project has received funding from the European Union's Horizon 2020 research and innovation programme under grant agreement No 769246 within the Stratospheric Flying Opportunities for High-Speed Propulsion Concepts (STRATOFLY) Project.

References

[1] Steelant, Johan. ATLLAS: Aero-thermal loaded material investigations for high-speed vehicles", 15th AIAA International Space Planes and Hypersonic Systems and Technologies Conference. 2008.
[2] Steelant, J., Varvill, R., Defoort, S., Hannemann, K., Marini, M.: Achievements Obtained for Sustained Hypersonic Flight within the LAPCAT-II Project, 20th AIAA International Space Planes and Hypersonic Systems and Technologies Conference, Glasgow, Scotland, AIAA- 2015-3677, 2015.
[3] E. Blanvillain, E. Gallic, "HIKARI: Paving the way towards high speed air transport", 20th AIAA International Space Planes and Hypersonic and Technologies Conference. Glasgow, Scotland, 2015.
[4] J. Steelant et al., "Conceptual Design of the High-Speed Propelled Experimental Flight Test Vehicle HEXAFLY", 20th AIAA International Space Planes and Hypersonic Systems and Technologies Conference, Glasgow, Scotland, 2015.

[5] N. Favaloro et al. “Design analysis of the high-speed experimental flight test vehicle HEXAFLY International”, 20th AIAA International Space Planes and Hypersonic Systems and Technologies Conference, Glasgow, Scotland, 2015.
[6] ICAO, "Annex 16 Volume I: Aircraft Noise." 2008
[7] ICAO, "Annex 16 Volume II: Aircraft Engine Emissions.", 2008
[8] ICAO, "Annex 16 Volume III: Procedures for the CO2 Emissions Certification of Aeroplanes, 2018
[9] Viola, N. & Fusaro, R., 2019. STRATOFLY MR3 vehicle configuration. Proc. Of the 25th Conference of the Italian Association of Aeronautics and Astronautics, 2019, Roma (IT), Springer.
[10] Marini M., Hernandez S., Saracoglu B.H., Ispir A.C., Lammers K., Natale P., Cutrone L., Roncioni P., Fusaro R., Viola N., “STRATOFLY Project Challenges in the Fields of Airframe, Aerothermodynamics, High-Speed Propulsion and Energy Management System”, International Conference on Flight Vehicles, Aerothermodynamics and Re-entry Missions and Engineering (FAR 2019), Monopoli, Italy, 30 September-3 October, 2019.
[11] J. Steelant, T. Langener, (2014) “The LAPCAT MR-2 Hypersonic Cruiser Concept” in 29th Congress of the International Council of the Aeronautical Sciences, St. Petersburg, Russia, 2014.
[12] Vincent-Randonnier A., Moule Y. & Ferrier M.; 2014, “Combustion of Hydrogen in Hot Air Flows within LAPCAT-II Dual Mode Ramjet Combustor at Onera-LAERTE Facility - Experimental and Numerical Investigation”, AIAA 2014-2931.
[13] Menon S. & Fureby C.; 2010, “Computational Combustion”, In Encyclopedia of Aerospace Engineering, Eds. Blockley R. & Shyy W., John Wiley & Sons.
[14] Zettervall N. & Fureby C.; 2018, “A Computational Study of Ramjet, Scramjet and Dual-mode Ramjet Combustion in Combustor with a Cavity Flameholder”, AIAA 2018-1146.
[15] Kim W.-W. & Menon S.; 1999, “An Unsteady Incompressible Navier-Stokes Solver for Large Eddy Simulation of Turbulent Flows”, Int. J. Num. Methods Fluids, 31, p 983.
[16] Sabelnikov V. & Fureby C.; 2013, “LES Combustion Modeling for High Re Flames using a Multi-Phase Analogy”, Comb. Flame, 160, p 83.
[17] Weller H.G., Tabor G., Jasak H. & Fureby C.; 1997, “A Tensorial Approach to CFD using Object Oriented Techniques“, Comp. in Physics, **12**, p 629.
[18] Hairer E. & Wanner G.; 1991, “Solving Ordinary Differential Equations”, II: Stiff and Differential-Algebraic Problems, 2nd Ed., Springer Verlag.
[19] Roncioni P., Natale P., Marini M., Langener T., Steelant J., “Numerical Simulations and Performance Assessment of a Scramjet Powered Cruise Vehicle at Mach 8”, Aerospace Science and Technology, Vol. 42, pp. 218-228, April–May 2015, http://dx.doi.org/10.1016/j.ast.2015.01.006.
[20] Y.B. Zel'dovič, “The Oxidation of Nitrogen in Combustion Explosions”, Acta Physicochimica 21, 577–628, (1946).
[21] C. J. Jachimowski, “An Analytical Study of the Hydrogen-Air Reaction Mechanism with Application to Scramjet Combustion”, NASA Technical Paper 2791, (1988).
[22] Hannemann K. & Martinez Schramm J.; 2007, “High Enthalpy, High Pressure Short Duration Testing of Hypersonic Flows”, In: Springer Handbook of Experimental Fluid Mechanics, p. 1081, Springer Berlin Heidelberg, Eds.: Tropea C., Foss J. & Yarin, A.
[23] Hannemann K., Martinez Schramm J. & Karl S.; 2008, “Recent Extensions to the High Enthalpy Shock Tunnel Göttingen (HEG)”, Proc. 2nd Int. ARA Days “Ten Years after ADS”, Arcachon, France, 21-23 October.
[24] Hannemann K., Martinez Schramm J., Laurence S. & Karl S.; 2015, “Shock Tunnel Free Flight Force Measurements using a Complex Model Configuration”, 8th European Symposium on Aerothermodynamics for Space Vehicles.
[25] Karl S. & Steelant J.; 2018, “Crossflow Phenomena in Streamline-Traced Hypersonic Intakes”, J. Prop. Power, 34, p 449.
[26] Le Texier et al., 1988, Q.J.R. Meteorol. Soc. 114, pp281-295; The role of molecular hydrogen and methane oxidation in the water vapour budget of the stratosphere.

[27] Leonov S. et al.; 2018, J. Prop. Power, Vol.34-2, Ethylene Ignition and Flameholding by Electrical Discharge in Supersonic Combustor, DOI: 10.2514/1.B36811.
[28] Vincent-Radonnier A. et al., 2014, AIAA – Aviation 2014, Atlanta (USA – Georgia), Combustion of Hydrogen in Hot Air Flows within LAPCAT-II Dual Mode Ramjet Combustor at Onera-LAERTE Facility - Experimental and Numerical Investigation, AIAA 2014-2931, DOI: 10.2514/6.2014-2932.
[29] Vincent-Randonnier A. et al., 2017, AIAA 55th AIAA Aerospace Sciences Meeting, Grapevine (USA –Texas), First experiments on plasma-assisted supersonic combustion at the LAERTE facility, AIAA 2017-1975, DOI: 10.2514/6.2017- 1975.
[30] Linke, F., "Environmental Analysis of Operational Air Transportation Concepts", Doctoral Thesis, Technical University of Hamburg, 2016.
[31] Fernández-Villace, V., Paniagua, G., & Steelant, J. (2014). Installed performance evaluation of an air turbo-rocket expander engine. Aerospace science and technology, 35, 63-79.
[32] Ispir, A. C., Gonçalves, P. M., & Saracoglu, B. H. (2019). Analysis of a combined cycle propulsion system for STRATOFLY hypersonic vehicle over an extended trajectory. In MATEC Web of Conferences (Vol. 304, p. 03001). EDP Sciences.
[33] Goncalves, P. M., Ispir, A. C., & Saracoglu, B. H. (2019). Development and optimization of a hypersonic civil aircraft propulsion plant with regenerator system. In AIAA Propulsion and Energy 2019 Forum (p. 4421).
[34] Verstraete, T., "CADO : a Computer Aided Design and Optimization Tool for Turbomachinery Applications," 2nd International Conference on Engineering Optimization, Lisbon, Portugal, 2010, pp. 1–10.
[35] Yunos, S. N. M. M., Ghafir, M. F. A., & Wahab, A. A. (2017, April). Aircraft LTO emissions regulations and implementations at European airports. In AIP Conference Proceedings (Vol. 1831, No. 1, p. 020006). AIP Publishing LLC.